Case History: Observed Liquefaction and its Evaluation after the April 16, 2016, M_w7.8 Muisne, Pedernales Earthquake

Xavier Vera-Grunauer, Sebastian Lopez, Oscar Gonzalez, Danilo Davila
Geoestudios S.A., Guayaquil, Ecuador
Sissy Nikolaou
WSP | Parsons Brinckerhoff, New York, USA
Jorge Ordoñez
Universidad de Especialidades Espíritu Santo, Guayaquil, Ecuador
Alvaro Aviles, Roberto Antón
Escuela Politécnica del Litoral, Guayaquil, Ecuador

ABSTRACT
The April 16, 2016 Muisne, Pedernales M_w 7.8 Earthquake in Ecuador caused significant damage to the northwest region of the country and widespread liquefaction through the Ecuadorian coast. The city of Manta, particularly its main commercial and touristic neighborhood, suffered severe liquefaction, which caused substantial damage to foundations due to post-liquefaction sand ejecta, shear-induced and volumetric deformations associate with ground failures, lateral spreading and ground subsidence. This paper presents a liquefaction evaluations based on SPT and CPTu tests in zones with observed surface manifestations but with no visible signs of liquefaction. The seismic demand and capacity for the liquefaction assessment were estimated from non-linear site response analyses based on actual recordings and soils properties derived from an extensive in-situ geotechnical and geophysical exploration program. Well-documented sites with associated damage and overall performance documentation provide useful information for worldwide geotechnical and liquefaction databases. The authors make recommendations for liquefaction-triggering curves specifically for the city of Manta based on the site-specific results and their comparison with the state-of-the-art liquefaction-triggering curves.

1 INTRODUCTION

The April 16, 2016, Muisne (Pedernales) earthquake, with a moment magnitude M_w7.8 struck the northwestern region of Ecuador leaving extensive damage throughout the Ecuadorian coast. As part of the country´s recovery, the Ministry of Urban Development and Housing (MIDUVI) hired the firm Geoestudios S.A. to develop geotechnical and seismic zonation in Tarqui, the densely populated neighborhood of Manta, one of the most affected cities. This paper presents highlights of the zonation efforts, including site characterization, liquefaction case histories, and regional liquefaction evaluation recommendations.

1.1 Studied Area

The city of Manta is located in the province of Manabí. It is one of the most important cities in the country, situated in a bay and has a deep-water port constituting one of the most important cities in the country. The neighborhood of Tarqui, shown on Figure 1, is a principal economic and touristic development center, and is the zone of interest for this document due to the high level of earthquake damage and extensive liquefaction manifestation.

2 GEOTECHNICAL EXPLORATION METHODS

The subsurface investigations included tests of standard Penetration (SPT) with Pile Driving Analyzer (PDA) energy measurements and Cone Penetration (CPTu).

Figure 1. Tarqui, Ecuador (Open Street Map, 2016).

The investigations integrated geophysical in-situ tests to measure the soil shear wave velocity V_s and determine the stratigraphy for site response analyses. These tests included Dynamic Penetration Cone Tests (DPT), Multi-Channel Analysis of Surface Waves (MASW) and Microtremor Array Measurements (MAM). Figure 2 shows locations and types of the Tarqui subsurface investigations with a total of 28 SPT tests and 25 CPTu tests. The liquefaction potential was evaluated for each test and the results were compared to physical evidence from field visits

of Geoestudios (Vera et al., 2017) and data from the Geotechnical Extreme Events Reconnaissance Association (Nikolaou et al., 2016). The compiled information was overlaid to high-resolution aerial photographs and satellite images taken 2 weeks after the earthquake.

3 CHARACTERIZATION OF TARQUI SITES

Figure 3 shows the 9 zones in which the Tarqui study area was divided, based on site characterization through field testing and geotechnical and geological characteristics. Soil dynamics criteria considered in this zonation included potential of sands to liquefy, clay cyclic degradation, and seismic risk in terms of foundation damage and stability. Zone 2 was considered as having no soil-induced structural damage according to Vera et al. (2017). The zones are:

- Zone 1. Sand and Clay Deposits, Cyclic Degradation
- Zone 2. Residual Soils, Hills
- Zone 3. Transition Zone Clay-Sand, Cyclic Degradation and Liquefaction in Sands
- Zone 4. Sand Deposits, Liquefaction in Sands
- Zone 5. Manta River Margins, Lateral Spreading
- Zone 6. Competent Granular Materials, Minor Damage
- Zone 7 and 8. Beach sands, Liquefaction in Sands
- Zone 9. Sand Deposits, Liquefaction in Sands

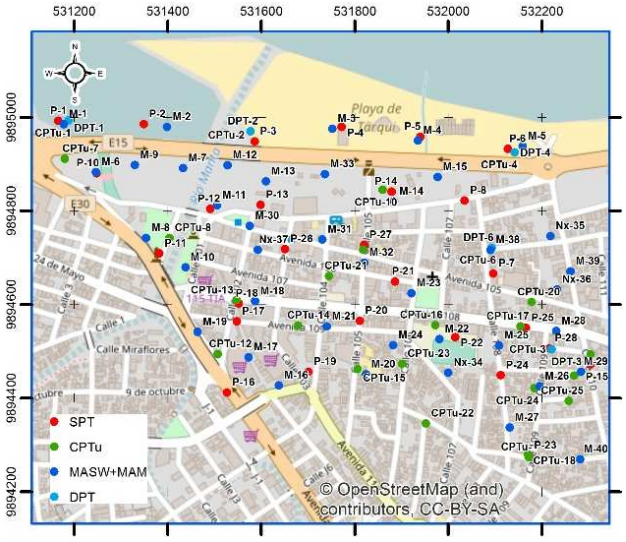

Figure 2. Subsurface investigation in the Tarqui study area.

4 GROUND MOTIONS

The April 16th, 2016, Muisne earthquake was recorded by a network of strong ground motion digital accelerometers throughout the country, which is managed and maintained by the National Accelerometer Network RENAC (Red Nacional de Acelerógrafos) (IGM, 2016).

This paper presents results obtained using input solely from the AMNT station in Manta. Table 1 presents the details of instrumentation, Peak Ground Accelerations and epicentral distance (Singaucho et al., 2016) for this station.

Figure 3. Zonation and SRAs of the Tarqui study area.

Table 1. AMNT station features (Singaucho et al., 2016).

Station	**AMNT**
City	Manta
Geographic Coordinates	Lat.: -0.941
	Lon.: -80.735
Elevation (m)	38
Instrument Type	Guralp
R_{rup} (km)	76
Vs_{30} (m/s)	496
PGA (g)	EW: 0.405
	NS: 0.524
	VER: 0.165

5 SITE RESPONSE ANALYSIS (SRA)

Figure 3 shows the locations were eight Site Response Analyses (SRA) were performed, using both effective and total stress approaches. The AMNT recorded acceleration time histories of the main event were the input in the SRAs. Since the AMNT station is not at outcropping rock, a deconvolution process determined the time histories at the hypothetical rock outcrop, used as SRA input.

The deconvolution process consists of inputting a known outcropping motion at the surface of a 1-D soil column and using an equivalent linear analysis to propagate this motion in order to estimate the time history within the underlying bedrock. This within motion can be converted to an outcropping motion and used as input in other site response analyses using characteristic soil columns (Kramer, 1996). The software SHAKE 2000 (Schnabel et al., 1972) was used for the deconvolution, considering the soil types present at the AMNT station. Based on in-situ measurements, a V_s profile was derived with values of 300 m/s to a depth of 3 m, 500 m/s from 3 to

22 m, reaching about 950 m/s at 22 m depth which was considered as characteristic for the rock halfspace.

Figure 4 shows a comparison of the 5%-damped acceleration response spectra (Sa) recorded at the AMNT station and those from the deconvolution for both the east (EW) and north (NS) horizontal components. The deconvoluted time histories were used in the SRAs performed on 8 characteristic soil columns based on the available field tests for each zone of Figure 3.

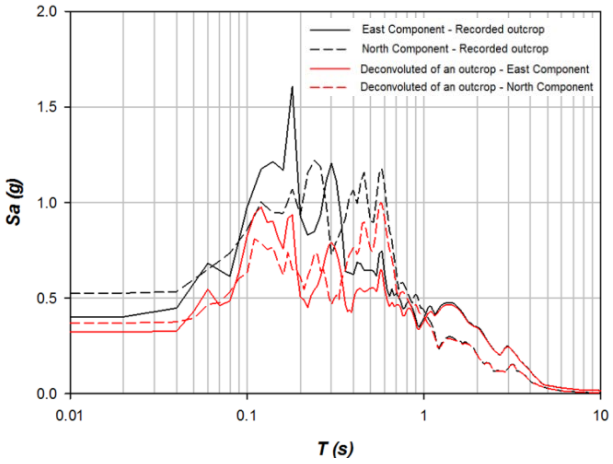

Figure 4. Acceleration spectra recorded (black) and obtained from deconvolution process (red).

Although the depth to the arcillolite bedrock varied, the soil profiles generally consisted of coarse-grained (loose to dense) and fine-grained (soft to stiff) layers. Stiffness degradation and hysteretic damping curves were assigned for each layer through curves proposed by Menq (2003) for sands and Darendeli (2001) for clays.

The SRAs were performed using Deepsoil (Hashash, et al., 2016), which contains an algorithm which evaluates the response of discretized systems, homogenous, visco-elastic of infinite extension, considering of shear waves in the vertical direction. It allows for nonlinear analysis in the time domain with or without pore pressure generation, and equivalent linear analysis in the frequency domain.

Figure 5 presents free-field acceleration response spectra for 5% structural damping in terms of effective and total stresses derived from Deepsoil.

6 LIQUEFACTION EVIDENCE AND MAPPING

To establish liquefaction-affected areas, a map was generated, which was based on field observations and high-resolution aerial photographs and satellite imagery taken 2 weeks after the earthquake. The map, shown on Figure 6, includes liquefaction evidence mainly expressed by ground cracking and sand boils on the ground surface, together with some actual ground failure images.

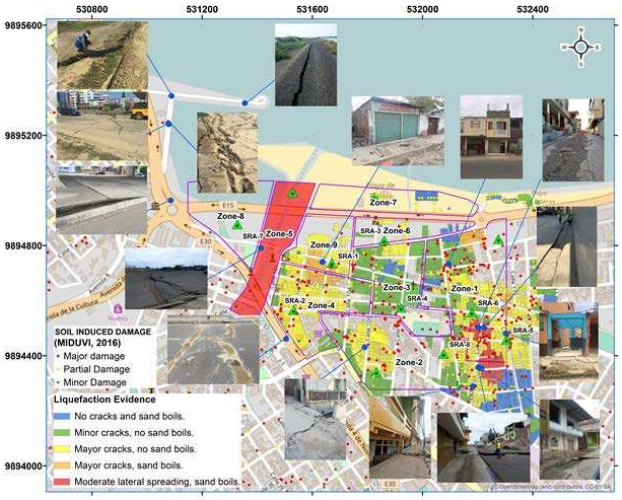

Figure 6. Compiled map of liquefaction evidence map through foundation and free field damage, together with photographic images of ground failures.

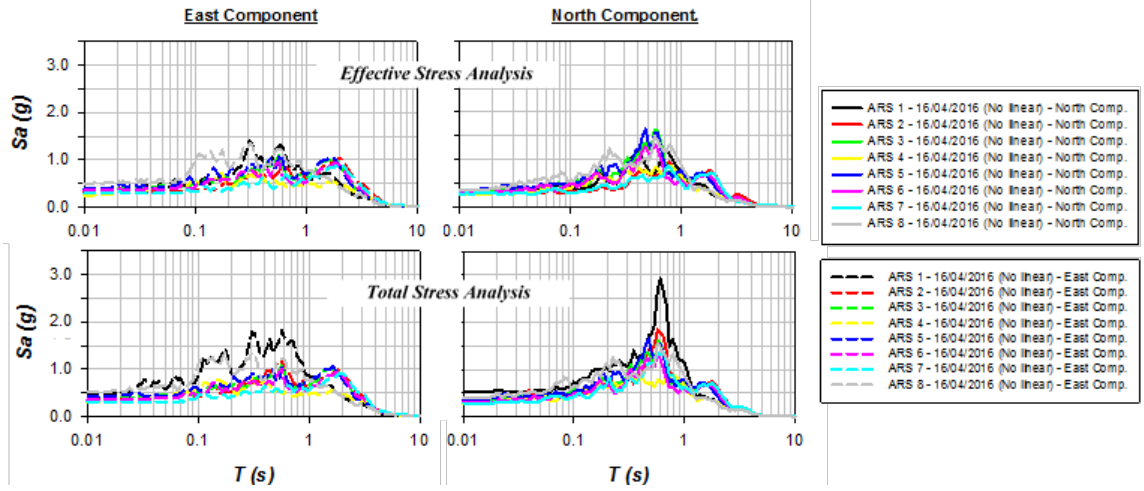

Figure 5. Acceleration response spectra for the 8 characteristic profiles obtained using Deepsoil in terms of effective and total stresses for a structural damping of 5% and free-field conditions.

7 LIQUEFACTION TRIGGERING POTENTIAL

Table 2 presents the SPT and CPTu field tests considered in the triggering analysis as valid sources of information with well-documented evidence of the liquefaction in the surface with locations shown on Figure. 2. In all tests considered, the water level was found at the time of the exploration at a depth of 2 to 3 m from the surface. Figures 7 and 8 present geotechnical parameters derived from these tests, including corrected blow counts for energy and overburden, $(N_1)_{60}$, and the fines content for the SPT, and the total cone tip resistance (q_t), friction ratio (F_r) and soil behavior type index (I_c), for the CPTu.

Table 2. Field tests used in liquefaction triggering analysis

SPT #		CPTu #	
Liquefaction	No Liquefaction	Liquefaction	No Liquefaction
P-10	P-8	CPTu-5	CPTu-10
P-11	P-14	CPTu-6	
P-15	P-19	CPTu-7	
P-26	P24	CPTu-8	
		CPTu-9	
		CPTu-11	
		CPTu-24	
		CPTu-25	

As a first screening, "critical" layers in each characteristic profile were identified using the in-situ test data and parameters of Figures 7 and 8, and physical evidence mapped on Figure 6. The depth and thickness of the layers evaluated are shown in Table 3. In the liquefaction cases, "critical" were the soil layers that were believed to have liquefied and caused surface manifestations. In the non-liquefaction cases, the range with lower N-values or cone tip resistance q_t was considered, adopting the average of these parameters.

Where fine soils were encountered, the Bray and Sancio (2006) criteria in the SPT-based evaluation was applied. In the particular case of SPT No. P-15, where high fines content may indicate clay, the liquefaction potential was evaluated in sand and silt layers detected throughout the profile and observed in the adjacent CPTu-9. Due to this mix of site conditions, it was considered that cyclic degradation of the clays could have also contributed to the observed ground damage.

Figure 9 shows laboratory results of grain size distribution curves for the SPT-based "critical" layers compared to the limits of liquefiable soils based on Tushida et al. (1970). The SPT tests where liquefaction was observed fit well between within the limits for most liquefiable soils, while for the sites where no liquefaction was observed, the gradation curves show a higher content of fine materials, being closer to the left boundary of the most liquefiable soils gradation curve.

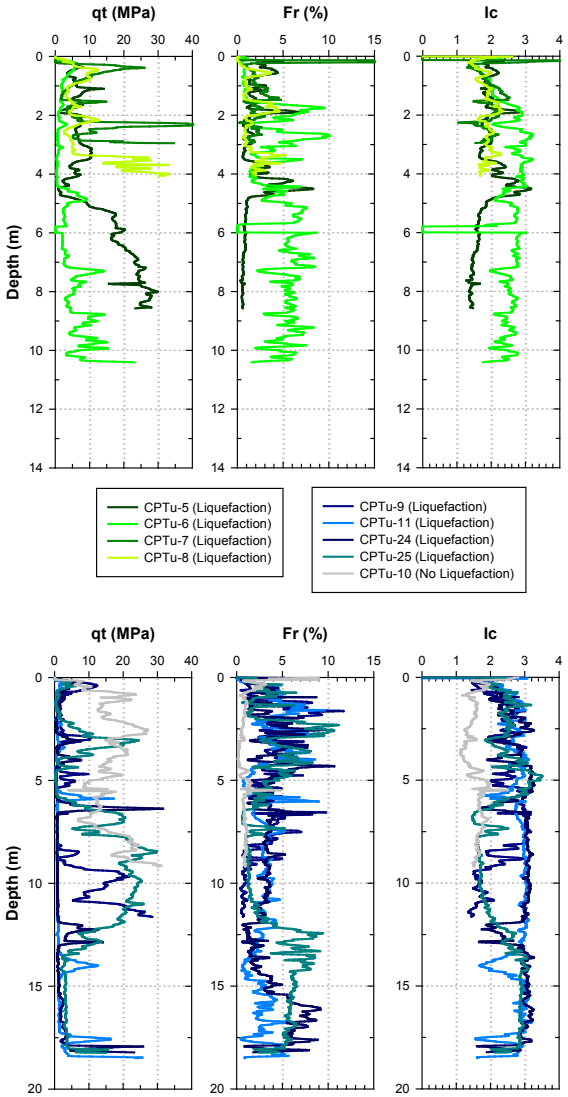

Figure 7. Geotechnical parameters from CPTu.

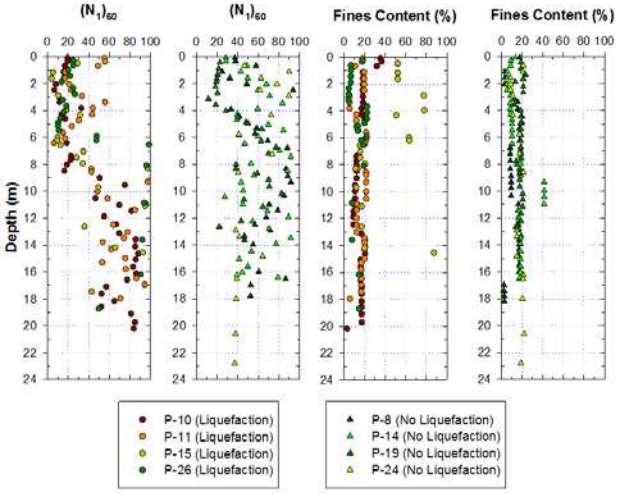

Figure 8. Geotechnical parameters from SPT.

Table 3. Thickness of liquefiable layers in SPT and CPTu.

	Test ID	Depth (m)	Thickness (m)
Liquefaction Evidence	P-10	2.30 - 8.70	6.50
	P-11	5.80 - 7.60	1.80
	P-15	5.80 - 6.80	0.50
	P-26	2.10 - 5.70	3.60
	CPTu-5	2.10 - 4.10	2.00
	CPTu-6	4.50 - 5.00	0.50
	CPTu-7	1.80 - 2.90	1.10
	CPTu-8	2.30 - 3.30	1.00
	CPTu-9	9.90 - 11.00	1.10
	CPTu-11	13.70 - 14.30	0.60
	CPTu-24	11.90 - 12.90	1.00
	CPTu-25	4.30 - 5.90	1.60
No Liquefaction Evidence	P-8	1.50 - 2.10	0.60
	P-14	10.00 - 11.00	1.00
	P-19	2.40 - 3.80	1.40
	P-24	11.50 - 12.50	1.00
	CPTu-10	5.00 - 7.50	2.5

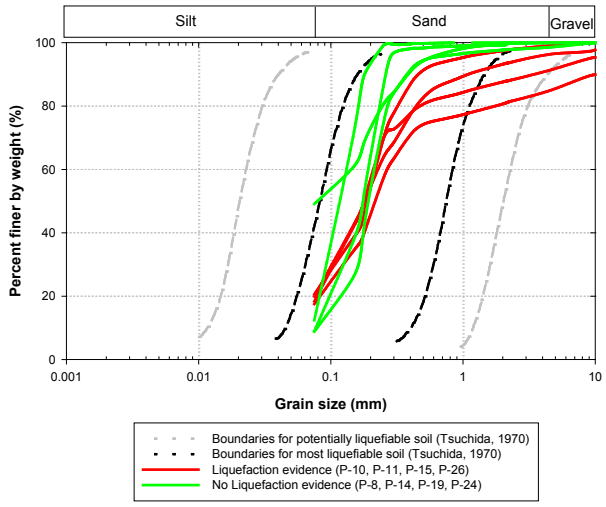

Figure 9. Grain size distribution limits for liquefiable soils compared to actual tests for critical layers in this study (modified from Tushida et al., 1970).

The earthquake-induced Cyclic Stress Ratio (CSR) was evaluated in terms of total stresses for the "critical" layers of the selected tests of Table 2. The empirical equation for CSR, originally derived by Seed & Idriss (1967) is shown on Equation 1. The dependence on the shaking intensity and duration and the effective overburden pressure, are expressed by the Magnitude Scaling Factor (MSF) and the K_σ factor, respectively.

$$CSR_{M=7.5,\,\sigma'_v=1} = 0.65\left(\frac{\tau_{max}}{\sigma'_v}\right)\left(\frac{1}{MSF\,K_\sigma}\right) \quad [1]$$

where: τ_{max} = maximum earthquake-induced shear stress and σ'_v = vertical effective stress. The subscripts indicate that CSR was scaled for an earthquake magnitude $M = 7.5$ through the MSF and normalized the in-situ σ'_v by 1 atm through the effective overburden stress factor K_σ.

The CSR values computed were plotted versus the CPT and SPT resistances corrected for overburden effects and expressed in terms of an equivalent clean-sand, $(N_1)_{60cs}$ and q_{c1Ncs}. Two methods, for both SPT and CPTu tests, were analyzed. The Boulanger & Idriss (2014) and Cetin et al. (2004) were applied for the SPT, and the Boulanger & Idriss (2014) and Moss et al. (2006) were used for the CPTu. The computational details are provided in the cited references. The results obtained using Equation 1 were compared with the CSR estimated by the Seed-Idriss (1967) simplified approach of Equation 2 (Boulanger & Idriss, 2014):

$$CSR_{M=7.5,\,\sigma'_v=1} = 0.65\left(\frac{\sigma_v}{\sigma'_v}\right)\left(\frac{a_{max}}{g}\right)\left(\frac{1}{MSF\,K_\sigma}\right)r_d \quad [2]$$

Where a_{max}/g = maximum horizontal acceleration, σ_v = vertical total stress, and r_d = shear stress reduction factor that accounts for the soil response with depth.

Figures 10 and 11 summarize the liquefaction evaluation results. Figure 10 includes triggering curves proposed by Idriss & Boulanger (2014) and Cetin et al. (2004) for SPT, and Figure 11 includes triggering curves proposed by Idriss & Boulanger (2014) and Moss et al. (2006) for the CPTu. While the main criteria followed, were the deterministic liquefaction triggering curves recommended by the referenced authors, the curves for the 50 and 85% liquefaction probabilities were also considered. Figure 12 shows a comparison between values computed using Equations 1 and 2.

8 DISCUSSION

As can be seen in Figures 10 and 11, the semi-empirical liquefaction triggering methodologies for both the SPT and CPTu tests that used the maximum earthquake induced shear stress derived from the SRAs generally match well the observations. The Boulanger & Idriss (2014) triggering method yields closer predictions to the field observations, while the Cetin et al. (2004) method seem to overestimate and the Moss et al. (2006) seem to underestimate the liquefaction potential as compared to the field data.

The Seed & Idriss (1967) simplified procedure tends to overestimate the earthquake-induced CSR, especially for higher demands, as shown on Figure 11. By considering the SRA in terms of effective stresses, the layers that liquefied were consistent with the "critical" layers defined from the SPT and CPTu tests. This comparison was made by assuming liquefaction when the excess water pressure ratio (R_u) became higher than 0.95 as described in detail in Vera et al. (2017).

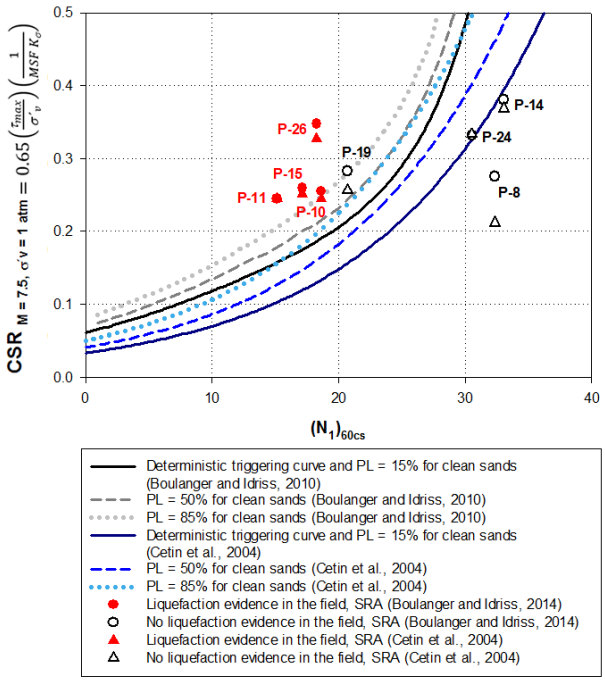

Figure 10. CSR vs. N-values corrected for overburden, and expressed in terms of equivalent clean sand $(N_1)_{60cs}$.

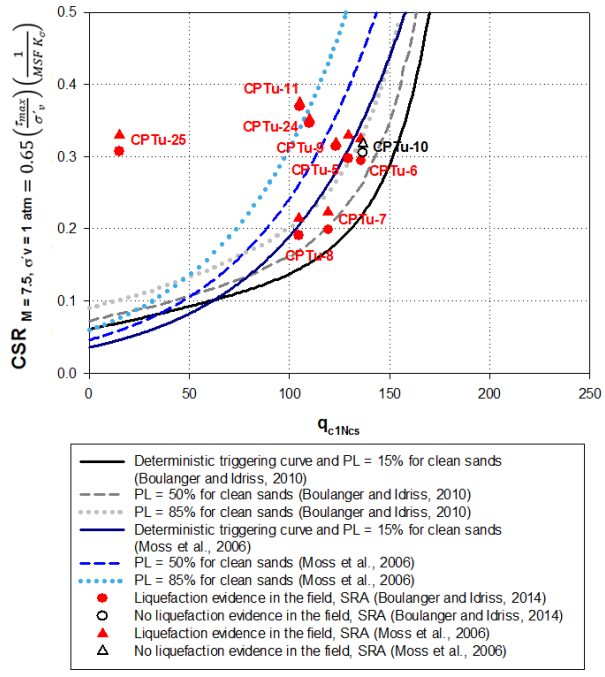

Figure 11. CSR vs. q_c-values corrected for overburden, and expressed in terms of an equivalent clean sand, q_{c1Ncs}.

Based on liquefaction triggering analyses and comparisons with widely used procedures in Manta, and particularly in Tarqui, the triggering curves proposed by Boulanger & Idriss (2014) appear to match better the observed behavior after the main event. However, further analyses are necessary to clarify the liquefaction vs. no-liquefaction boundary.

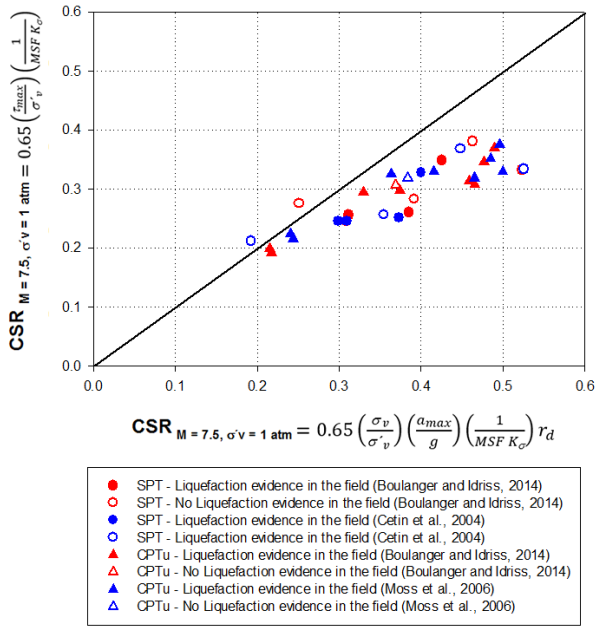

Figure 12. CSR values computed using Equations 1 and 2.

9 SUMMARY AND CONCLUSIONS

This paper presented soil liquefaction evaluation based on in-situ CPTu and SPT tests performed in the area of Tarqui in the city of Manta, in Ecuador. The results to observed ground manifestations of liquefaction at the test locations shortly following the April 16, 2016, Muisne (Pedernales) earthquake were compared. Semi-empirical, widely used liquefaction triggering methodologies were able to capture well most of the observed field behavior, which was also verified with effective stress site response analyses. From the various methods, the Boulanger & Idriss (2014) provided better match and would be recommended for use of further applications in this study area.

The extend of the geotechnical and geophysical testing, combined with the analytical studies conducted and the comparisons with well-documented observations in the field can be used to enhance world-wide SPT and CPTu liquefaction databases.

10 ACKNOWLEDGEMENTS

The Ecuadorian Ministry of Urban Development & Housing (MIDUVI) funded the testing and seismic zonation of Tarqui performed by Geoestudios S.A. of Guayaquil. Field information was partially based on the Geotechnical Extreme Events Reconnaissance Association's GEER-049 report "GEER-ATC Earthquake Reconnaissance: April 16 2016, Muisne, Ecuador." This work was supported by the National Science Foundation through Grant CMMICMMI-1266418. The GEER Association is made possible by the vision and support of the NSF Geotechnical Engineering Program Directors: Dr. Richard Fragaszy and the late Dr.

Cliff Astill. GEER members donate their time, talent, and resources to collect time-sensitive field observations after extreme events. Financial contribution from the Applied Technology Council (ATC) supported the participation of two structural engineers and US agencies, academic institutions, engineering firms and individuals volunteered with time and resources. Other information and assistance provided by the Ecuadorian Ministry of Transportation & Public Works, the Geophysical Institute, the 911 Emergency Agency, the Army Polytechnic School (ESPE), and the Army Corps of Engineers (ECACE).

11 REFERENCES

Boulanger, R.W., Idriss, I.M. (2010). SPT-based liquefaction triggering procedures. Rep. UCD/CGM-10.

Boulanger, R.W., Idriss, I.M. (2014). CPT and SPT based liquefaction triggering procedures. Center for Geotechnical Modeling, UC Davis.

Bray, J.D., Sancio, R.B. (2006). Assessment of the liquefaction susceptibility of fine grained soils. J. of Geotechnical & Geoenv. Eng., ASCE, 132(9):1165-77.

Cetin, K.O., Seed, R.B., Der Kiureghian, A., Tokimatsu, K., Harder, L.F. Jr., Kayen, R., Moss, R. (2004). SPT-based probabilistic & deterministic assessment of seismic soil liquefaction potential. J. of Geotechnical and Geoenv. Engineering, ASCE, 130(12):1314-40.

Darendeli, M.B. (2001). Development of a new family of normalized modulus reduction and material damping curves, Department of Civil Engineering, UT Austin.

Nikolaou, S., Vera-Grunauer, X., & Gilsanz, R., eds., 2016. GEER-ATC Earthquake Reconnaissance: April 16 2016, Muisne, Ecuador, Rep. GEER-049, co-authors: Alvarado, A., Alzamora, D., Antonaki, N., Arteta, C., Athanasopoulos, A., Bassal, P., Caicedo, A., Casares, B., Davila, D., Diaz, V., Diaz-Fanas, G., Gilsanz, R., González, O., Hernandez, L., Kishida, T., Kokkali, P., López, P., Luque, R., Lyvers, G.M., Maalouf, S., Mezher, J., Miranda, E., Morales, E., Nikolaou, S., O'Rourke, T., Ochoa, I., O'Connor, J., Ripalda, F., Rodríguez, L.F., Rollins, K., Stavridis, A., Toulkeridis, T., Vaxevanis, E., Villagrán León, N., Vera-Grunauer, X., Wood, C., Yepes, H., Yepez, Y. Available at geerassociation.org.

Google Inc., 2016. Google Earth Pro (Version 7.0.2.8415) [Software]. Mountain View, CA.

Hashash, Y.M.A., Musgrove, M.I., Harmon, J.A., Groholski, D.R., Phillips, C.A., and Park, D. (2016) "DEEPSOIL 6.1, User Manual".

Instituto Geofísico at Escuela Politécnica Nacional, IG-EPN, 2016a. Acelerógrafos, Publicado en Instrumentación, igepn.edu.ec/acelerografos, last accessed 7/1/16.

Kramer, S. (1996). Geotechnical Earthquake Engineering. Prentice Hall, NJ.

Menq, F-Y (2003). Dynamic properties of sandy & gravelly Soils, Department of Civil Engineering, UT Austin.

Moss, R., Seed, R.B., Kayen, R., Stewart, J.P., Der Kiureghian, A., Cetin, K.O. (2006). CPT-based probabilistic and deterministic assessment of in situ seismic soil liquefaction potential. J. of Geotechnical & Geoenv. Engineering, ASCE, 132(8):1032–1051.

Schnabel, P.B., Lysmer, J., Seed, H.B. (1972). "SHAKE: A computer program for earthquake response analysis of horizontally layered sites," Report UCB/EERC-72/12, Earthquake Eng. Res. Center, UC Berkeley, 102 p.

Seed, H.B., Idriss, I.M. (1967). "Analysis of liquefaction: Niigata earthquake." Proc., ASCE, 93(SM3), 83-108.

Seed, H.B., Idriss, I.M. (1971). "Simplified procedure for evaluating soil liquefaction potential." J. Soil Mechanics & Foundations Div., ASCE 97(SM9), 1249-1273.

Seed, H.B., Idriss, I.M. (1982). Ground motions and soil liquefaction during earthquakes, EERI Earthquake Eng. Research Institute Monograph, Oakland, 134 p.

Singaucho J.C., Laurendeau A., Viracucha C., Ruiz M., (2016). Observaciones del sismo del 16 de Abril de 2016 de magnitud M_w7.8, Intensidades y Aceleraciones, Sometido a la Revista Politécnica.

Tsuchida, H. (1970). Prediction and countermeasure against the liquefaction in sand deposits. Abstract, Seminar in Port & Harbor Research Institute, pp. 3-1.

Vera-Grunauer, X., Lopez, S., Davila, D., Vargas, J., Ordoñez, J., Ramirez, J., Vera, A., Tituaña, J., Aviles, A., Antón, R. (2017). Geotechnical and Seismic Risk Study of the Tarqui Area of the City of Manta in Accordance with the 2015 Ecuadorian Construction Standard. Ministry of Urban Development and Housing.